Non-Native Heme−Histidine Ligation Promotes Microsecond Time Scale Secondary Structure Formation in Reduced Horse Heart Cytochrome *c*†

Eefei Chen,* Christina J. Abel, Robert A. Goldbeck, and David S. Kliger

Department of Chemistry and Biochemistry, University of California, Santa Cruz, California 95060

Received April 17, 2007; Revised Manuscript Received July 5, 2007

ABSTRACT: Previous far-UV time-resolved optical rotatory dispersion (TRORD) studies of the submillisecond (burst) phase of secondary structure formation in horse and tuna cytochromes *c* after photoreduction in denaturant suggested that the non-native His18-Fe-His33 heme ligation dominant in the unfolded horse protein facilitated this fast folding better than did the His18-Fe-His26 coordination dominant in tuna [Chen, E., Goldbeck, R.A., and Kliger, D.S. (2003) *J. Phys. Chem. A 107,* 8149−8155; Chen, E., Goldbeck, R.A., and Kliger, D.S. (2004) *J. Am. Chem. Soc. 126,* 11175−11181]. Whether His18-Fe-His33 coordination actually facilitates fast secondary structure formation or just slows folding less than His18-Fe-His26 coordination is probed by examining the double histidine mutant H26QH33N of horse heart cytochrome *c*. The fast folding phase is absent in H26QH33N, indicating that His18-Fe-His33 misligation does promote fast secondary structure formation, as does His18-Fe-His26 to a lesser extent. His33 may be better able to facilitate folding because it is not as constrained by hydrogen bonding interactions in the denatured state as is His26. A greater flexibility, not only because of weakened or disrupted Van der Waals interactions in the presence of guanidine hydrochloride (GuHCl) but also because of its position relative to His18, may allow His33 to ligate to the heme group more easily than His26. These results are discussed along with the results of far-UV CD and Soret and visible region MCD measurements, which were performed to probe heme ligation in H26QH33N and to understand how GuHCl affects its folding stability and cooperativity.

The folding kinetics of reduced cytochrome *c* (redcyt *c*[1]) have been studied in the presence of the denaturant guanidine hydrochloride (GuHCl) for both the horse heart and tuna heart species of the protein (*1*−*13*). The results of time-resolved circular dichroism and time-resolved optical rotatory dispersion (TRORD) electron-transfer-triggered folding studies on horse heart redcyt *c* report two major folding phases on time scales faster and slower than a millisecond (*6*, *11*, *12*). The slow folding phase is characterized by reaction kinetics that become slower with increasing denaturant concentration. This folding behavior is consistent with the expectation that the free energy of activation is proportional to the decrease in the driving force. The rates observed during the slow phase are in the same time region detected by the stopped-flow CD measurements that have been used to explore the dynamics of secondary structure formation in oxidized cytochrome *c* (oxcyt *c*) (*14*).

In striking contrast, the kinetics of the fast, "burst" phase in horse heart redcyt *c* showed greater amplitude and more rapid formation of secondary structure with increasing GuHCl concentration. Specifically, on going from 3.3 to 4 M GuHCl, more secondary structure was formed within hundreds of nanoseconds during the fast folding phase. The different effects of denaturant on this phase versus the slow phase of horse heart redcyt *c* suggested that they undergo fundamentally different folding processes. The appearance and behavior of the fast phase was indicative of kinetic heterogeneity, which is observed in the earliest events of horse heart redcyt *c* folding wherein protein-backbone conformational and heme−ligand binding heterogeneities are the greatest (*11*). This time frame corresponds to the top of the protein folding funnel, where the unfolded conformers can either equilibrate with each other (around the periphery of the funnel) or start to fold (down the length of the funnel). The competition between the folding and the conformational diffusion kinetics determines whether folding follows a sequential (homogeneous/classical TST) or a parallel (heterogeneous/new view) mechanism. The results of recent time-resolved magnetic optical rotatory dispersion studies of CO-bound H26Q, H33N, and H26QH33N mutants of redcyt *c* indicate that the time required for unfolded conformers to interconvert is 3 ± 2 μs (*15*). This relatively long interconversion time constant explains why it was possible to observe folding within several hundred nanoseconds from a fast-folding conformational subensemble in the presence of a larger slow-folding component in the horse heart protein. The fast-folding component was effectively kinetically isolated from the slow component by slow conformational equilibration.

The heterogeneity introduced to the bulk protein structure of cyt *c* by denaturant leads to competition between the native

† Supported by National Institutes of Health Grant EB02056.

* To whom correspondence should be addressed. Phone: (831)459-4007. Fax: (831)459-2935. E-mail: chen@chemistry.ucsc.edu.

[1] Abbreviations: redcyt *c*, reduced cytochrome *c*; GuHCl, guanidine hydrochloride; TRORD, time-resolved optical rotatory dispersion; oxcyt *c*, oxidized cytochrome *c*; cyt *c*, cytochrome *c*; CD, circular dichroism; MCD, magnetic circular dichroism.

10.1021/bi7007273 CCC: $37.00
Published on Web 10/03/2007

heme axial ligand Met80 and non-native ligands. At the 3.3 and 4 M GuHCl concentrations used in the horse redcyt *c* TRORD studies, the bis-His (His18-Fe-His33/26) heme configuration was shown to be the dominant ferric heme ligation (*16*−*19*). In order to understand the role of His33/26 in the kinetic heterogeneity observed in horse heart redcyt *c* folding (*11*, *20*), the dynamics of redcyt *c* folding in tuna heart, wherein the His33 is replaced by a Trp moiety, were studied with TRORD methods. As with the horse heart protein, two phases were observed for tuna heart redcyt *c* folding in 3.3 and 4 M GuHCl. However, the rise time that is characteristic of fast phase secondary structure formation in horse heart redcyt *c* slowed considerably (from hundreds of nanosecond to tens of microseconds) and was accompanied by less secondary structure formation in tuna redcyt *c*. These differences in the folding kinetics of the fast phase are interesting in light of the similarities in the native structures, stabilities, and unfolding free energies for the horse heart and tuna heart proteins.

Out of the 20% amino acid residues that differ between the two species, the presence of His33 in the horse heart protein is expected to have the largest effect on the dynamics of folding. In this regard, the decreased amplitude of the fast folding phase in the tuna heart data offered insights into the source of the kinetic heterogeneity observed in horse redcyt *c*. The amplitude of the fast folding phase in horse heart redcyt *c* corresponds to about 20% of the native secondary structure in redcyt *c*. The coincidence of this 20% fast folding amplitude and the 20% His18-Fe-His26 minor constituent of the total heme ligations in the presence of GuHCl (*18*), suggested that the fast folding subpopulation may simply correspond to the His18-Fe-His26 coordination. However, the absence in tuna heart redcyt *c* of the very fast folding phase observed in horse heart redcyt *c* ruled out this alternative explanation for the heterogeneous folding kinetics in horse redcyt *c* and implied that the His18-Fe-His33 heme ligation was a requirement for very fast folding. Moreover, this requirement appears to be necessary but not sufficient because 80% of the protein chains have the His18-Fe-His33 heme coordination (whereas the fast folding phase amplitude is 20%).

The results of these previous TRORD studies on horse heart and tuna heart redcyt *c* folding lead to the question of whether the His18-Fe-His33 heme ligation facilitates secondary structure formation or does it just slow folding less than the His18-Fe-His26 coordination. This question is probed here with far-UV TRORD measurements of redcyt *c* folding in the horse heart double mutant (horse H26QH33N), where both His26 and His33 are removed. Far-UV CD and Soret and visible region MCD experiments were also performed to probe the heme ligation configuration in the horse H26QH33N cyt *c* protein, as well as to understand how GuHCl affects the stability and cooperativity of its folding process.

MATERIALS AND METHODS

Mutant Genes Construction and Expression and Protein Purification. Mutations to the horse heart cyt *c* gene contained in the modified plasmid pBRT1 (*21*, *22*) were made using the Quickchange Site-directed Mutagenesis Kit (Stratagene, La Jolla, CA). The mutant gene was verified by sequencing the plasmid DNA.

As described previously (*21*, *23*), the H26QH33N cyt *c* mutant was expressed in tandem with yeast heme lyase in BL21(DE3)pLysS (*Escherichia coli*) cells (Invitrogen, Carlsbad, CA). A single colony containing the H26QH33N mutant was used to inoculate 25 mL of Luria Broth containing 100 μg/μL ampicillin. After incubation at 37 °C overnight and vigorous shaking (200−250 rpm), the culture was used to inoculate 1 L of Terrific Broth (MP Biomedicals, Irvine, CA) containing 100 μg/μL ampicillin. Protein expression was induced by addition of 0.8 mM IPTG at A_{600} between 0.8 and 1.0. Expression was carried out at 37 °C for 24−36 h with shaking at 225−250 rpm. After centrifugation of the cultures at 8000 rpm for 20 min, the resulting cell pellets were lysed by adding lysis buffer containing 50 mM Tris, 1 mM EDTA, 10 mM $MgCl_2$, 3 g/L lysozyme, and 20 μg/mL DNaseI at pH 7.5. Next, the cells were French pressed two times at 15000 psi. After spinning for 20 min at 8000 rpm, the supernatant was subjected to an ammonium sulfate precipitation by adding ammonium sulfate to 55% (326 g/L). Next, the sample was centrifuged (20 min, 8000 rpm) and the supernatant was dialyzed against several changes of 25 mM sodium phosphate buffer, pH 7.5 at 4 °C overnight. Then the protein solution was loaded onto a cation-exchange column (CM Sepharose, Amersham Biosciences), which was equilibrated with 25 mM sodium phosphate buffer, pH 7.5. After several washes of 25 mM sodium phosphate buffer, the protein was eluted using a linear NaCl gradient from 40 mM to 250 mM and collected in 4 mL fractions. Fractions that had an $A_{410}/A_{280} > 4.0$ were pooled, dialyzed against several changes of water, and lyophilized. Mass spectrometry (Ettan MALDI-ToF/Pro instrument, Amersham Biosciences) confirmed the mutant protein.

Sample Preparation. WT horse heart oxcyt *c* and NADH from Sigma-Aldrich (St. Louis, MO), sodium phosphates (NaP; monobasic and dibasic) from Thermo Fisher Scientific (Waltham, MA), sodium hydrosulfite (dithionite) from Fluka Chemicals (Ronkonkoma, NY), and ultrapure GuHCl from MP Biomedicals (Costa Mesa, CA) were used without further purification.

For the TRORD experiments on oxidized H26QH33N cyt *c*, samples were prepared in enough 0.1 M NaP−3.3 M GuHCl buffer (pH 7) to obtain an absorption value at 404 nm of 0.8−0.9 in a 1-mm path length cell. The oxcyt *c* solution was first stirred in air to oxidize trace redcyt *c* and then deoxygenated with nitrogen gas for about 15 min. At the same time a vial containing enough NADH solid to obtain a 500 μM concentration in the final cyt *c* solution was placed in a glovebag that was continuously purged with nitrogen gas. When ready the deoxygenated oxcyt *c* solution was placed into the glovebag and added to the solid NADH. UV−vis spectra (UV-2101PC spectrophotometer, Shimadzu, Columbia, MD) of the samples were measured before and after addition of the NADH. The GuHCl concentrations in the oxcyt *c* solution and in the pure buffer were determined from their refractive index values, which were measured on a refractometer (ABBE-3L, Milton Roy). Equilibrium ORD spectra of oxcyt *c* and redcyt *c* were obtained on the same sample as those used for the TRORD measurements. Redcyt *c* was prepared by adding dithionite to the oxcyt *c* solution. A UV−vis spectrum of the redcyt *c* sample was acquired prior to the ORD measurements to check for complete conversion of oxcyt *c*.

The samples for equilibrium Soret and visible region MCD and far UV CD measurements were prepared by making stock solutions of WT horse heart and horse H26QH33N oxcyt *c* (~85 μM and ~20 μM for the measurements, respectively) in 0.1 M NaP without denaturant (pH 7) and in 0.1 M NaP with ~6 M GuHCl (pH 7). These solutions were mixed in appropriate aliquots to obtain oxcyt *c* samples in 3.3 M GuHCl (pH 7) for the MCD experiments and in 1.1, 1.8, 2.3, 2.6, 3.1, 3.6, 4, 4.4, 4.6, 4.7, and 5.9 M GuHCl for the far UV CD experiments. MCD spectra for oxcyt *c* and redcyt *c* in the 0.1 M NaP and 0.1 M NaP−6 M GuHCl stock solutions were accumulated in both spectral regions. For both MCD and CD samples, the pH was readjusted to 7 after mixing the two stock solutions and the refractive index values were obtained to determine the GuHCl concentration. Redcyt *c* samples were prepared by adding dithionite to deoxygenated oxcyt *c* solutions. They were then loaded into a 1-mm quartz cuvette that was sealed with a ground glass stopper or a screw cap. These steps for preparation of redcyt *c* were performed in a glovebag filled with nitrogen gas. UV−vis spectra of the oxcyt *c* and redcyt *c* samples were collected before the MCD and CD measurements, and for redcyt *c*, a second UV−vis spectrum was collected at the completion of the measurement.

Time-Resolved ORD Experiments. The rapid oxidation of NADH was initiated by 355-nm pulses (~15 mJ, 7 ns, full-width half-maximum) generated by a Quanta Ray DCR-1 Nd:YAG laser. The subsequent reduction of oxcyt *c* triggered protein folding, the time-dependence of which was followed spectrally with the TRORD apparatus. In that apparatus, the xenon flash lamp probe beam passed through a MgF_2 polarizer and a UV-enhanced aluminum spherical mirror (F2/ Edmund Optics) before it reached the sample, where it overlapped with the photoexcitation beam. The 355-nm beam was focused down to a spot size of 1−2 mm, whereas the spherical mirror focused the probe beam to a diameter of ~300 μm. Subsequently, the probe beam continued through a second UV-enhanced aluminum spherical mirror and a second MgF_2 polarizer before it was focused onto the slit of a spectrograph that was dispersed with a 600 grooves/mm grating (200-nm blaze). The probe beam was detected by a CCD (iStar, Andor Technology, South Windsor, CT). ORD signals were measured by rotating the first polarizer by angles of $+\beta$ and then $-\beta$ off the crossed position (90°) of the two polarizers. The ORD signal is the ratio of the difference between the $+\beta$ and $-\beta$ intensities and the sum of the intensities. In these experiments, $\beta = 1.87$ °. For further details about the TRORD apparatus readers are directed to the article by Shapiro et al. (*24*).

TRORD data for redcyt *c* folding were measured at 500 ns, 1.5, 4, 10, and 100 μs, 1, 10, 50, and 100 ms after photoexcitation. About 840 averages were collected at 1.5 μs and 312 to 376 averages were accumulated at all other time delays. Measurements were taken every 2 s and sample was flowed only between laser shots. The flow rate was 8−9 μL/s, a rate that was sufficient to prevent build-up of photoproduct or photodegraded products. The deoxygenated oxcyt *c* sample (in 0.1 M NaP−3.3 M GuHCl and 500 μM NADH) was moved with a peristaltic pump from a flask in the nitrogen-purged glovebag to a 1-mm path length flow cell that was constructed with quartz windows. After irradiation the sample was flowed out to a collection vial where it was regenerated for further TRORD experiments. The integrity of the sample was determined by UV−vis measurements, specifically, the visible bands were used as monitors for the appearance of small concentrations of redcyt *c*. The sample was maintained at a temperature of 25 °C and the temperature was checked periodically throughout the experiment with an infrared temperature probe (80T-IR, Fluke). GuHCl concentrations and the pH of the samples were measured before and after the experiments.

Equilibrium ORD signals were obtained on the TRORD apparatus. For oxcyt *c*, spectra were measured along with each time-delayed measurement; redcyt *c* was prepared and measured at the end of the experiments.

Equilibrium MCD and CD Experiments. Far UV CD spectra were measured on a CD spectrophotometer (AVIV model 60DS, Lakewood, NJ). Data were collected every 1 nm with a 1-nm bandwidth from 190 to 300 nm using a 1-mm path length rectangular quartz cuvette. These data were measured with an integration time of 8 s at each step. For MCD measurements, a 0.64 T PM-2 permanent magnet (JASCO Inc., Easton, MD) was placed in the sample compartment of the CD spectrophotometer. A 1-mm path length circular quartz cuvette was positioned between the two poles of the magnet. Data were collected every 1 nm with an integration time of 8 s (1-nm bandwidth) for the two different orientations of the magnetic field, parallel and antiparallel to the propagation direction of the light beam. MCD data were measured between 350 and 600 nm and MCD spectra were calculated as half the difference of the signals obtained in the parallel and antiparallel magnetic field configurations.

Data Analysis. The TRORD data were analyzed in the form of difference ORD signals obtained by subtracting the time-resolved signals from the initial oxcyt *c* signal. Although the data are collected as multichannel signals, exponential fitting analyses were performed on kinetic traces that were calculated by averaging the multichannel data from 229 to 235 nm. Analysis algorithms were written in the mathematical software package Matlab (The MathWorks, Inc., South Natick, MA). Data points on the H26QH33N far UV CD folding titration were determined by calculating the fraction of unfolded protein at each concentration of GuHCl relative to the native, fully folded (0 M GuHCl) and the "fully unfolded" (6 M GuHCl) protein. The fractional secondary structure content was calculated using the difference ORD signal measured at each time delay and the difference ORD signal for the final folded (redcyt *c*) state. The intensities of the CD signal at 220 nm for each concentration of denaturant was determined by averaging the data from 215 to 225 nm.

RESULTS

MCD of Oxidized cyt c. To understand the heme environment and ligation state of the initial, largely unfolded oxidized horse H26QH33N species and the reduced horse H26QH33N photoproduct, equilibrium MCD experiments in the Soret to visible regions (350−650 nm) were performed on these samples in the presence of denaturant and in the native state. The results of these experiments are shown in Figure 1 (oxidized) and Figure 2 (reduced). Figure 1a normalizes and overlays the Soret MCD spectra of the native oxidized WT horse heart and horse H26QH33N. They have

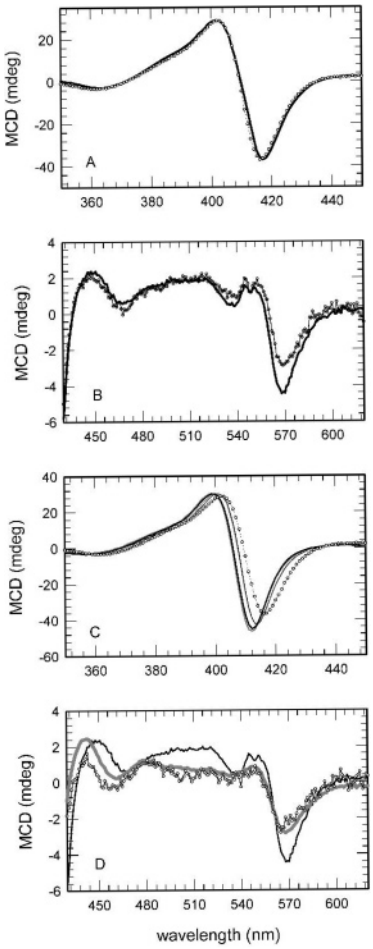

FIGURE 1: MCD spectra of oxidized WT horse heart and horse H26QH33N in the native and denatured states. (A) The Soret MCD spectrum for native WT horse heart (solid black line) is overlaid with the native horse H26QH33N (thin black line with open circles) spectrum. The spectra are normalized at the positive MCD feature. The same spectra are shown in the 430 to 620 nm region in part B. The MCD spectra for horse H26QH33N when it is denatured in 3.3 M GuHCl (thick gray line) and in 6 M GuHCl (thick black line) are shown in part C. These denatured horse H26QH33N MCD spectra are blue-shifted from the spectra of the WT horse heart protein denatured in 3.3 M (thin gray line) and in 6 M GuHCl (thin black line), as well as from the native horse H26QH33N (thin black line with open circles). Because the spectra for the WT protein in 3.3 and 6 M GuHCl overlay, the thin gray line is obscured by the thin black line. In part D, MCD spectra in the 430 to 620 nm region are shown for native WT horse heart oxcyt *c* (thin black line), horse H26QH33N oxcyt *c* in 3.3 M GuHCl (thin black line with open circles), and native WT horse heart oxcyt *c* at pH 10 (thick gray line). The spectra are normalized at the ca. 400 nm band. All samples are at pH 7 unless otherwise noted.

the same band shapes and about the same band intensities, but the positive band (ca. 402 nm) is slightly broader for the WT horse spectrum. The negative band (416 nm) for the horse double mutant is about 1 nm blue-shifted from the same band for the WT horse heart. In Figure 1b, the spectra of the same species shown in Figure 1a are very similar in the 480 to 520 nm region, a region that is diagnostic of the heme ligand coordination (*25*, *26*), but the band at 570 nm is less intense for the horse H26QH33N spectrum. Whereas these results suggest that the heme ligation of His18-Fe-Met80 found in WT horse heart is preserved in native horse H26QH33N, they also suggest that the heme interaction with the surrounding polypeptide is similar but weaker in the

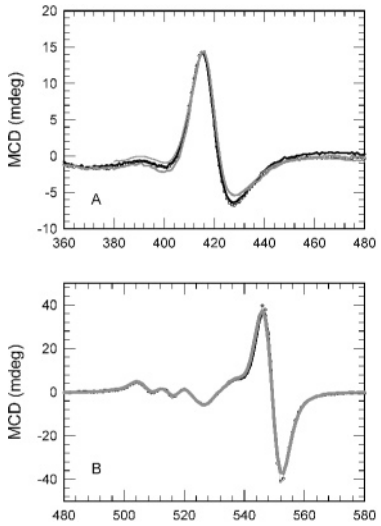

FIGURE 2: MCD spectra of reduced WT horse heart and horse H26QH33N in the native state and in denaturant. In part A, the Soret MCD spectra for native horse H26QH33N redcyt *c* (thin black line with open circles), native WT horse heart redcyt *c* (thick black line), horse H26QH33N redcyt *c* in 3.3 M GuHCl (thick gray line), and WT horse heart redcyt *c* in 3.3 M GuHCl (thin gray line). The spectra are normalized to the MCD maximum band at ca. 416 nm and are clearly very similar to each other. These same spectra are shown in part B, but in the visible region.

double mutant. A similar decrease at the 570 nm MCD band was observed for the GuHCl-unfolded WT horse heart oxcyt *c* relative to the native protein by Thomas et al. (*19*).

When denatured in 3.3 M GuHCl (Figure 1c), the WT horse heart protein exhibits a positive (ca. 401 nm) and a negative (412 nm) band that are blue-shifted from the bands of the native proteins (Figure 1a). The MCD spectrum for the WT horse heart in 6 M GuHCl can be overlaid with that measured in 3.3 M GuHCl. For the horse H26QH33N protein in 3.3 M GuHCl, the MCD spectra are further blue-shifted from the WT horse heart native (Figure 1a) and denatured bands. The spectrum of horse H26QH33N in 6 M GuHCl can also be overlaid with the MCD spectrum obtained in 3.3 M GuHCl. The similarities between the MCD spectra of the two proteins in 3.3 and 6 M GuHCl indicate that in 3.3 M GuHCl they are already in their "fully unfolded" state. Figure 1d compares the native WT horse heart protein at pH 7 with denatured horse H26QH33N (3.3 M GuHCl) in the 430−530 nm region. This comparison suggests that the heme ligation in denatured horse H26QH33N is not the native His18-Fe-Met80 coordination. When the MCD spectrum of denatured horse H26QH33N is overlaid with the spectrum of the WT horse heart protein at pH 10, where the sixth axial ligand is proposed to be Lys (*27*, *28*), there is a much closer match. Thus, the initial denatured (in 3.3 M GuHCl) horse H26QH33N oxcyt *c* sample that is used for the TRORD experiments has a protein conformation that is "fully unfolded" and a heme coordination that is tentatively assigned to His18-Fe-Lys. Although the His18-Fe-Lys coordination has been observed previously for cyt *c* in both urea (*29*) and GuHCl (*30*), the MCD data here cannot definitively preclude the coordination of the N-terminus to the heme without an MCD spectrum of this heme ligation state. Studies by Hammack et al. suggest that under denaturing conditions (3 M GuHCl) the N-terminal amino group will coordinate with the heme moiety in pH regions where

non-native heme ligations have largely been attributed to the His ligand (*31*). Although the N-terminus is not acetylated in H26QH33N as it is in the WT horse heart and tuna heart proteins, the good overlay of the MCD spectra in Figure 1d suggest that the percentage of any heme-N-terminus coordination is either very small or absent. The discrepancy in the non-native ligation states between the results by Hammack et al., and these MCD results may arise from the differences in the denaturing conditions. The difference between 3 and 3.3 M GuHCl has been shown in denaturant titrations of cyt *c* to account for as much as 20% unfolded secondary structure and may thus also account for the observation of the two different heme ligations. This would be consistent with the denaturant concentration dependence of the heme ligation state that was observed previously for the His18-Fe-His and His18-Fe-Lys denatured forms (*30*).

MCD of Reduced cyt c. The Soret MCD spectra of the reduced horse H26QH33N protein (Figure 2a) have two major lobes, ca. 416 and 428 nm, and a minor lobe at ca. 400 nm. The MCD spectra (normalized at 416 nm) of the native WT horse heart at pH 7 and the native horse H26QH33N redcyt *c* proteins and their denatured (in 3.3 M GuHCl) counterparts can be overlaid. A comparison of the spectra in the visible region for the same species is shown in Figure 2b. The visible MCD spectrum for the native WT reduced horse heart protein at pH 7 is characterized by a positive 547-nm band and a negative 552-nm band. When the intensities of the MCD spectra are normalized at the main, 416-nm Soret band the features in the visible region can also be overlaid. The MCD spectra shown in Figures 2a and 2b were also compared to the MCD measurement of WT horse heart redcyt *c* at pH 10 (data not shown). When normalized in the Soret region, the MCD spectrum of the WT horse heart redcyt *c* at pH 10 can be overlaid with the spectra in Figure 2a. However, the spectrum in the visible region was greater in intensity and slightly (∼1 nm) blue-shifted relative to the spectra shown in Figure 2b. Overall, these MCD data suggest that at 3.3 M GuHCl, the protein environment around the heme chromophore is native-like in horse H26QH33N redcyt *c*. That is, the heme coordination of the horse H26QH33N redcyt *c* is apparently His18-Fe-Met80/Met65.

Denaturant Titration. Figure 3a compares the unfolding curve for the oxidized and reduced H26QH33N cyt *c* as a function of GuHCl concentration with those for the WT horse heart and tuna heart cyt *c* proteins. The unusual shape for H26QH33N is interpreted not as an intermediate of protein unfolding, but as an indication of sample heterogeneity. Supporting data for this conclusion are based on a comparison of the concentration calculated from a known weight and volume of protein and the concentration calculated from the heme absorption of the UV−vis spectrum. The difference in the calculations indicated that there was about 55% apocyt *c* present in the initial oxcyt *c* solutions. The presence of the apocyt *c* proteins will not affect the TRORD data because only the oxcyt *c* molecules will undergo photoreduction. Consequently, the contribution of apocyt *c* to the ORD signal before and after the photoreduction trigger is the same and is subtracted out because the data are analyzed in the form of difference spectra. However, the apocyt *c* is a problem for equilibrium measurements. Because apocyt *c* is present in both the oxidized and reduced solutions the overlap of the data at GuHCl concentrations less than 2.5 M is attributed

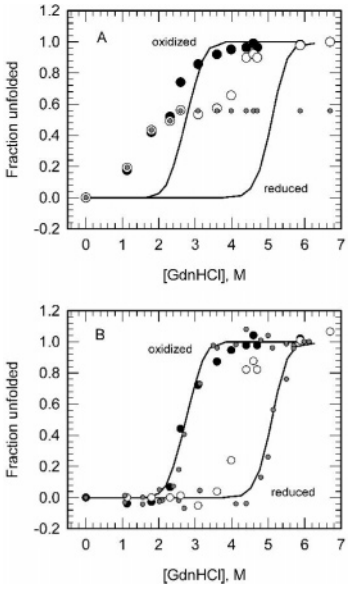

FIGURE 3: GuHCl titration of oxidized (large black circles) and reduced (large white circles) horse H26QH33N. In part A, these unfolding titration curves are compared to those for WT horse heart (solid lines). The measured data shows unusual behavior for the oxidized and particularly the reduced H26QH33N secondary structures as a function of increasing concentrations of GuHCl. The rise at early denaturant concentrations for both the H26QH33N oxcyt *c* and redcyt *c* unfolding curves and the plateau observed in the latter between 2 and 4 M GuHCl are attributed to unfolding of an ensemble of apocyt *c*. A correction for the contribution of apocyt *c* (small gray circles) is estimated based on the expected unfolding curves for WT horse heart redcyt *c*. The folding curves are corrected by subtracting the estimated contribution due to apocyt *c* and are shown in part B and compared with the curves for WT horse heart (black lines) and WT tuna heart (small gray circles).

to unfolding of the apocyt *c* subpopulation. It is noted that apocyt *c* is reportedly largely disordered (*32*, *33*), although studies of a synthetic C-terminal peptide suggested that it was possible for apocyt *c* to have some residual helical structure (*34*). Because the unfolding titration curve for WT horse heart and WT tuna heart redcyt *c* have C_m values of ∼5 M GuHCl, an assumption is made that for H26QH33N redcyt *c* unfolding will not occur at denaturant concentrations less than about 3 M GuHCl, where the early unfolding process has already plateaued. Thus, because apocyt *c* is destabilized by concentrations of denaturant that are significantly lower than that required to unfold redcyt *c*, the unfolding titration curve for the apocyt *c* is known and can be subtracted from the measured titration curves to extract the unfolding titration curve for pure H26QH33N redcyt *c*. Because apocyt *c* is unaffected by the dithionite that is used to convert oxcyt *c* to redcyt *c*, it should be possible to use the estimated apocyt *c* unfolding data obtained from the redcyt *c* curve to correct the oxcyt *c* unfolding titration trace. The corrected unfolding titration curves are shown in Figure 3b. The C_m for oxidized H26QH33N does not differ from that for the WT horse heart or tuna heart proteins. However, for redcyt *c* H26QH33N, the C_m value decreases by about 1 M GuHCl.

Kinetics of H26QH33N Redcyt c Folding. The kinetic trace obtained from the TRORD experiments on horse H26QH33N redcyt *c* folding in 3.3 M GuHCl is shown in Figure 4a relative to the kinetic trace for WT horse heart redcyt *c* folding in the same GuHCl concentration. Figure 4a shows

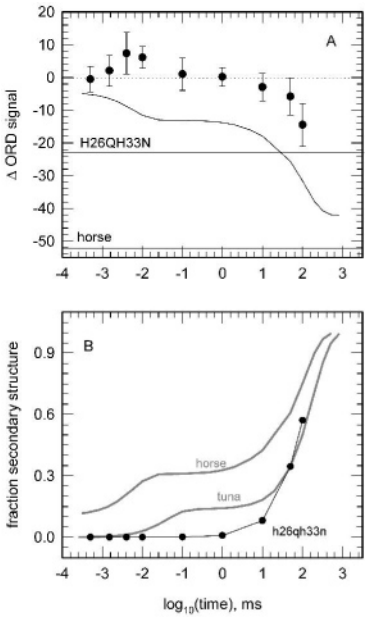

FIGURE 4: Kinetics of horse H26QH33N redcyt *c* folding triggered by rapid photoreduction. In part A, the time evolution of the difference ORD signals for horse H26QH33N (black circles) and WT horse heart (black line) redcyt *c* folding in 3.3 M GuHCl are compared. The equilibrium ORD signals for the wild type horse heart and double mutant proteins are shown as solid lines. Part B compares the kinetics for WT horse heart (gray line), WT tuna heart (gray line), and horse H26QH33N (black circles). The experimental data points are shown along with the fit to the data ($\tau = 120$ ms).

the TRORD signals for horse H26QH33N redcyt *c* folding at 500 ns, 1.5, 4, 10, and 100 μs, and 1, 10, 50, and 100 ms after the initial photoreduction event. With the exception of the 4 and 10 μs time points, the behavior of the kinetic trace indicates that there is no unfolding up to approximately 1 ms. The time points at 4 and 10 μs show a further decrease in secondary structure, relative to oxcyt *c*, that is probably artifactual because the initial, oxidized starting material is already ~88% unfolded (Figure 3b). Although the unfolding titration curves in Figure 3b suggest that 12% secondary structure remains folded at 3.3 M GuHCl, it is likely to be due to the correction applied to account for the presence of apocyt *c* (see above). This is supported by the MCD data which suggest that at 3.3 M GuHCl the protein is fully unfolded because the spectrum can be overlaid with that measured in 6 M GuHCl. In addition, the changes in the ORD signal at these time points are too abrupt and cannot be fit to a first-order kinetic process. Thus, the rapid phase of folding (<1 ms) that is evident in the WT horse heart redcyt *c* folding trace disappears in the horse H26QH33N redcyt*c* data. The smaller redcyt *c* ΔORD signal for H26QH33N relative to the signal for WT horse heart is attributed to the fact that the concentration of oxcyt *c* was smaller than expected because of the contribution of apocyt *c*.

A comparison of the fraction of secondary structure that forms as a function of time is shown in Figure 4b for WT horse heart, WT tuna heart, and horse H26QH33N redcyt *c*, all in 3.3 M GuHCl. The data at 4 and 10 μs are assumed to show no secondary structure changes (see above), as is true for the three other data points (500 ns, 1.5 and 100 μs) measured before 1 ms. Consequently, the fraction secondary structure is set to zero at 4 and 10 μs for this Figure. In this figure, it is clear that the successive removal of the possible non-native heme ligands, His33 and H26, decreases the amplitude and rate of secondary structure formation. The rise time for the fast phase secondary structure formation in horse heart redcyt *c* ($\tau \sim 2$ μs) slows significantly for the tuna protein. Whereas substantial secondary structure forms within several hundred nanoseconds for the WT horse heart redcyt *c*, the WT tuna heart redcyt *c* does not begin to fold until after ~5 μs and has a 40 μs time constant of folding in this fast phase. For horse H26QH33N redcyt *c*, the kinetic trace exhibits only a single (slow, >1 ms) phase. A comparison of the signals in Figure 4b shows that the dynamics of the slow phase in H26QH33N is about the same as that for the WT proteins. That is, 75% and 50% of the WT horse heart and tuna heart redcyt *c* proteins have folded by 100 ms, and 58% of the H26QH33N protein is folded by that time. Because only a few time points were measured during the rise of the slow folding phase, the fit of the data to 120 ms is an estimate of the time constant. The slow phase of folding has been correlated with formation of the native secondary structure. In the case of the WT horse heart and tuna heart proteins, this would first involve displacement of the non-native His ligands with the native Met80 moiety (*18*). The MCD experiments discussed in Figure 1 suggest that the native, Met80 moiety is not the sixth axial ligand in the initial, oxidized H26QH33N sample. Rather, the data show spectral similarity between oxcyt *c* H26QH33N in 3.3 M GuHCl and oxcyt *c* WT horse heart at pH 10, indicating the presence of a Lys group. Consequently, in this slow phase a Lys residue would have to be displaced by Met80 in order to achieve the final folded redcyt *c* structure. The slow phase is not discussed in detail because the focus of this study was the fast folding phase.

DISCUSSION

Redcyt *c* folding can be initiated using ligand photodissociation (*1*) and electron transfer (*2*−*4*), two methods that rely on the differences in the folding free energies of the oxidized, reduced, and CO-bound reduced proteins in the presence of denaturant. The oxidized, CO-bound reduced, and reduced proteins are >95% unfolded in GuHCl concentrations above 3, 4, and 5 M, respectively. Thus, in the approximate denaturant range of 3−5 M, it is possible to trigger folding of the reduced protein from the largely unfolded, either CO-bound reduced or oxidized, starting material. Although the photodissociation method is limited by CO recombination in its ability to capture secondary and tertiary structure formation, it can provide details of protein folding on the nanosecond and tens of microsecond time scale. A relatively large (hundreds of nanoseconds to 1 s) window on protein folding is available, however, with the rapid electron-transfer trigger. Both triggers have been used to initiate folding in the tuna heart and in the wild type and various mutants of the horse heart redcyt *c* proteins (*1*−*6*, *8*−*13*).

The unusual kinetics that have been observed on the submicrosecond time scale in the results of far-UV TRORD studies of electron-transfer triggered redcyt *c* folding have been attributed to conformational heterogeneity of the initial unfolded protein chains (*11*, *20*). On the hundreds of nanoseconds time scale, where this kinetic heterogeneity is the most dramatic, the heterogeneity of the polypeptide-

backbone configuration is the greatest. On this time scale, different unfolded ensembles do not yet undergo equilibration, which has been reported to occur with a time constant of 3 ± 2 μs (*15*), and so can evolve independently of one another. The very rapid formation of secondary structure observed in WT horse heart redcyt *c* folding has been attributed to a small subpopulation of the total unfolded polypeptide chains that is conformationally poised to fold (*11*).

From TRORD studies of folding in WT horse heart and tuna heart cyts *c*, it was proposed that a structural necessity for this small unfolded ensemble to undergo fast folding is that the protein chains must have the His18-Fe-His33 heme configuration. However, because the His18-Fe-His33 ligation makes up 80% of the unfolded protein chains (*18*) and the amplitude of the fast phase is 20%, having this heme coordination alone will not lead to fast folding. Whereas those TRORD results eliminated heme ligand heterogeneity as the source of the kinetic heterogeneity, they did not establish what role the His18-Fe-His33 heme coordination played in fast folding. That is, does it facilitate fast folding or does it just slow down fast folding less than the His18-Fe-His26 ligation? This question is explored in the present study with TRORD measurements on the horse H26QH33N redcyt *c* protein, where both non-native His ligands are removed. Soret and visible MCD data were obtained to interrogate the ligation states of the starting oxidized solution and the final folded reduced material.

Folding Titrations and Heme Ligations of Oxidized and Reduced H26QH33N. Unlike the single mutants, H33N and H26Q, where the CD-detected unfolding titration curves indicate that removal of either one of the two His residues has small destabilizing effects on the folding stability of the protein (*35*), the corrected unfolding titration for H26QH33N (Figure 3b) overlays that for WT horse heart cyt *c* (*12*). The discrepancy in the stabilities of the single and double mutants relative to the WT protein may arise from the estimate of the contribution of apocyt *c* to the unfolding curves. This correction may also explain the differences in the H26QH33N and WT horse unfolding curves in the concentration range between 3 and 4 M GuHCl. The absence of the two His residues that play a major role in the equilibrium heme coordination of WT horse heart oxcyt *c* in the presence of denaturant raises the question of whether the native Met80 ligand is similarly displaced by an alternate non-native ligand in horse H26QH33N. An attempt here to use MCD spectroscopy to identify the heme coordination in the initial, oxidized starting material suggests that in the presence of 3.3 M GuHCl the sixth axial ligand is not the native Met80 residue. In 3.3 M GuHCl the protein conformation is largely unfolded, as demonstrated by the Soret MCD (Figure 1c). According to Russell et al. (*30*), the His18-Fe-Lys (residues 79, 72, or 73) axial coordination is detected for oxidized WT horse heart in 1.5−2.3 M GuHCl. However, at higher GuHCl concentrations (2.3−8 M GuHCl) His33/26 is found at the sixth axial site. In 3.3 M GuHCl, the absence of both His moieties makes Lys a good candidate for axial coordination in denatured oxidized horse H26QH33N. This assignment appears consistent with the MCD spectral features for denatured horse H26QH33N in the 430−530 nm region (Figure 1d), which are less characteristic of the His18-Fe-Met80 coordination than is apparent in the native horse H26QH33N protein (Figure 1b). From a comparison of the MCD data for the denatured oxidized horse H26QH33N and for the WT horse protein at pH 10, the heme ligation is assigned here to His18-Fe-Lys. This comparison tentatively rules out the possibility of the ligation of the N-terminal group, which in the H26QH33N is not acetylated (*18*, *23*).

In contrast to the unfolding curve for oxidized H26QH33N the data for the reduced form shows a clear shift of unfolding toward lower concentrations of GuHCl. The data suggests that whereas H26QH33N redcyt *c* is destabilized relative to WT horse heart redcyt *c*, removal of the two non-native histidines does not affect the folding cooperativity. The difference in the redcyt *c* denaturant titration curves may be explained by the stabilizing effect of the His18-Fe-His heme ligation in WT horse heart relative to the His18-Fe-Met coordination, suggested here by MCD experiments, in horse heart H26QH33N. The denaturant titration for oxidized H26QH33N was also expected to shift toward lower GuHCl concentrations relative to the curve for the WT horse heart protein. The coincidence of those titration curves is interesting in light of the small, but distinct, destabilization observed for the H33N and H26Q single mutant denaturant unfolding curves when compared to that for the WT protein (*18*, *35*). This discrepancy may be due to the correction applied to remove the contribution of apocyt *c* from the denaturant titration curve. The error in the estimate of the apocyt *c* denaturant-dependent unfolding curve may be large enough to obscure any destabilization due to the absence of both His residues.

Fast Folding Kinetics of H26QH33N Redcyt c Folding. Upon fast photoreduction of the initial, unfolded oxidized horse H26QH33N sample in 3.3 M GuHCl, the immediate photoproduct is the reduced form with largely unfolded protein (>90%) and a putative His18-Fe-Lys heme configuration. Subsequent folding of reduced horse H26QH33N involves the ~44% subpopulation of the sample that contains the heme group (vide infra) and displacement of the Lys residue by a Met ligand at the heme group. In this study the folding process was followed by far-UV TRORD methods from 500 ns until only 100 ms because the focus of these studies was on the fast folding phase (<1 ms). When compared to the results of similar studies on WT horse heart redcyt *c*, the fast phase of folding is absent for the horse H26QH33N redcyt *c* protein. With removal of His33, as in WT tuna heart redcyt *c*, the fast folding process is smaller in amplitude, as well as in rate constant (*12*). That result for WT tuna heart redcyt *c* eliminated the possibility of simple ligation-based heterogeneity (i.e., the His18-Fe-His26 minor component in WT horse heart cyt *c*) as the origin of the fast folding phase and suggested that the presence of His33 was a necessary but not sufficient requirement for the fastest submillisecond folding. The absence of the fast folding phase in the H26QH33N results presented here suggests that His18-Fe-His33 heme ligation facilitates fast folding in an absolute sense and that it does so more than does the His18-Fe-His26 coordination. For the alternative hypothesis where His18-Fe-His33 would slow fast folding less than His18-Fe-His26, the fast folding phase in horse H26QH33N redcyt *c* would have exhibited faster dynamics than for either of the two WT redcyt *c* proteins.

What clues do the TRORD kinetic results for reduced horse H26QH33N folding provide to improve our under-

standing of the fast phase folding dynamics in horse WT and tuna WT redcyt *c*? The relatively independent behavior of the two His residues during the fast folding phase for the two WT species, i.e., the different kinetics observed when His18-Fe-His33 (horse heart) or His18-Fe-His26 (tuna heart) coordination is dominant, is inconsistent with the suggestion of close communication between the two by the similar effect on the fluorescence-detected equilibrium folding titration curves for two oxidized single mutants, H26Q and H33N (*18*, *35*). In horse heart cyt *c*, a comparison of the C_m values of these two oxidized forms (H26Q, $C_m = 2.54$ M; H33N, $C_m = 2.44$ M) with that for the WT ($C_m = 2.61$ M) indicates that the removal of either one of the two His residues has only small destabilizing effects on the folding stability relative to the WT protein. In contrast, the TRORD kinetic data indicate that His33 plays a more significant role than His26 in the fast folding phase. The different results of the kinetic versus equilibrium studies are consistent with the results of previous studies which suggest that the factors that facilitate fast folding may be decoupled from the factors that influence the protein native structure and stability (*36*, *37*). Detection of the slower and smaller amplitude fast folding phase in WT tuna heart redcyt *c* suggests that, in the absence of His33, His26 alone cannot maintain the structural requirements for fast folding.

The structural elements most readily associated with the two His residues are a β-turn (residues 21−24) and the carboxy-terminal residue of the protein backbone (*38*), which are linked by Van der Waals interactions with His33, and two Ω-loops (20s and 40s) that are bridged by His26 via two H-bonds (triad H-bond network) to Pro44 and Asn31. Although mutations at His26 in rat cyt *c* (H26V (*38*)) and in yeast iso-1-cyt *c* (H26Y (*39*)) have demonstrated a significant reduction in protein stability that is suggested to result from an increased flexibility of the Ω-loops due to weakening or breaking of the triad H-bond network (*23*, *38*, *40*), modeling studies of WT horse heart and the H26Q mutant demonstrate that this H-bond network is maintained even with the glutamine substitution at His26 (*41*). Further, NMR studies of the WT horse heart and tuna heart oxcyt *c* indicate that the triad H-bond network is still formed even at denaturant concentrations of 7 M GuHCl (*42*). Thus, at 3.3 M GuHCl the triad H-bond network in WT tuna redcyt *c* is expected to be intact, which may explain why the His26 residue cannot compensate for the absence of His33 in tuna WT redcyt *c* in terms of heme ligation. That is, the His26 may be restricted in its mobility by the two H-bonds and may be unable to form a productive heme ligation to facilitate a significant amount of folding on that time scale. In this regard, His33 may be able to facilitate folding because it is 'anchored' not by H-bonding interactions but by weaker Van der Waals interactions (*38*). Thus, a greater flexibility, not only because of weakened or disrupted Van der Waals interactions in the presence of GuHCl but also because of its relative position to His18, may allow His33 to ligate to the heme group much more rapidly and easily than His26.

The relative position of His26 and His33 to His18 and the ability to form a loop with the heme group may play a significant role in the formation of secondary structure in the fast phase. Fundamentally, the sequence composition of the residues between His18 and His26/33 suggests that there is a greater propensity for a loop formed by His33 versus His26 ligation to the heme because of the presence of one more glycine and a proline in the former (*43*−*46*). Further insights into the structural differences between His33 and His26 in the capacity of loop formation are offered by studies of the tendency of different parts of denatured iso-1-cyt *c* protein to coordinate with the heme. Although the pK_a(obs) values for the His26 and His33 variants are the same within the error of the measurement, in contrast to the apparent pK_a reported for His26 (6.1) and His33 (5.7) in horse heart cyt *c* (*18*), there are modest differences in the residual structure (∼1 kcal/mol) and the heme affinity (∼5-fold increase) for the His33 variant relative to the His26 variant when the His18-Fe-His33/26 loop is formed (*43*). The formation of simple loops is important to a basic understanding of the earliest events in protein folding. Measurements of loop formation rates under denaturing conditions provide information on the relative probability and sequence composition for different-sized loops. Studies of heme−His loop formation and breakage using stopped-flow absorption methods report a general correlation between increasing rates of formation and decreasing loop size (*36*). Although the smallest loop size studied was 10, extrapolation of the data to a loop size of 9 gives a rate of formation for the His18-Fe-His26 loop that is greater than that for His18-Fe-His33. The time constants calculated from these rates are generally consistent with the time constant reported for transient binding of His26 and His33 to the heme group (*10*). Perhaps even more important, however, is the rate of loop breakage, which will determine the likelihood that an initial loop will persist and lead to efficient folding. For reduced horse heart cyt *c*, the expectation is that the size of the loop formed by His26 ligation to the heme is too transient to facilitate formation of the secondary structure detected in these far-UV TRORD studies. According to Kurchan et al. (*36*), for small loop sizes of less than 37 the rate of breakage does not exhibit a regular trend. For example, chain stiffness is expected to play a significant role in breakage of small loops, yet the size 16 loop has a slower rate of breakage than the size 22 loop. The irregularity of the breakage rates suggest that other factors besides loop size are involved. Thus, it appears that for WT tuna heart redcyt *c* the previously discussed idea that the His18-Fe-His26 configuration is hindered by the short distance between His18 and His26 may be only one explanation for why it might have a smaller driving force for helix formation during this phase. An additional factor, beyond loop stiffness, that has been offered as a reason that His26 has a lower affinity for the heme is the presence of surrounding Lys residues (Lys25 and Lys27) that lead to charge repulsion with the iron (*43*).

That there is biological significance for a protein misligation is counterintuitive in light of the significance of a proper fold toward functional successes on the cellular level. For redcyt *c*, the importance of His33 has been demonstrated in solution structure studies of the protein in 30% acetonitrile/70% water (*47*). This medium has a low dielectric constant ($\epsilon = 67$) that mimics the environment of the mitochondrial membrane (lipid vesicles, $\epsilon = 30-60$). According to that study, redcyt *c* shows a significant decrease in the solvent accessible surface area, which includes His33, compared with its structure in aqueous media. His33 undergoes a significant conformational change (whereas His26 does not) in order to accommodate the environment of the membrane, which

may help to preserve the specificity of the electron-transfer pathways. In this regard, perhaps His33 helps to regulate the secondary structure content in order to facilitate the protein−membrane interaction. The flexibility of His33 and its involvement in protein folding may have biological significance for the physiological roles played by cyt *c*. Its most recognized function is as a membrane protein that shuttles electrons in the mitochondrial respiratory pathway (*48*, *49*). More recently, cyt *c* has been shown to be involved in apoptosis, which requires that cyt *c* be transferred across the mitochondrial membrane into the cytosol (*50*). Its incorporation into and transport across membrane highlight the importance of the unfolded or partly unfolded conformations to its function. Protein dynamics in the presence of mimetic membranes such as anionic surfactants and lipid membranes have shown that interactions with natively folded cyt *c* results in partial unfolding, whereas interactions with unfolded cyt *c* leads to partial refolding of the protein (*51*−*54*). Thus, understanding how His33 facilitates folding, even in the presence of denaturant, may contribute to understanding how cytochrome *c* achieves its varied functions at the cellular level.

ACKNOWLEDGMENT

We thank George McLendon for the generous gift of the plasmid pBRT1.

REFERENCES

1. Jones, C. M., Henry, E. R., Hu, Y., Chan, C.-K., Luck, S. D., Bhuyan, A., Roder, H., Hofrichter, J., and Eaton, W. A. (1993) Fast events in protein folding initiated by nanosecond laser photolysis, *Proc. Natl. Acad. Sci. U.S.A. 90*, 11860−11864.
2. Mines, G. A., Pascher, T., Lee, S. C., Winkler, J. R., and Gray, H. B. (1996) Cytochrome *c* folding triggered by electron transfer, *Chem. Biol. 3*, 491−497.
3. Pascher, T., Chesick, J. P., Winkler, J. R., and Gray, H. B. (1996) Protein folding triggered by electron transfer, *Science 271*, 1558−1560.
4. Telford, J. R., Wittung-Stafshede, P., Gray, H. B., and Winkler, J. R. (1998) Protein folding triggered by electron transfer, *Acc. Chem. Res. 31*, 755−763.
5. Chen, E., Wood, M. J., Fink, A. L., and Kliger, D. S. (1998) Time-resolved circular dichroism studies of protein folding intermediates of cytochrome *c*, *Biochemistry 37*, 5589−5598.
6. Chen, E., Wittung-Stafshede, P., and Kliger, D. S. (1999) Far-UV time-resolved circular dichroism detection of electron-transfer-triggered cytochrome *c* folding, *J. Am. Chem. Soc. 121*, 3811−3817.
7. Bhuyan, A. K., and Udgaonkar, J. B. (2001) Folding of horse cytochrome *c* in the reduced state, *J. Mol. Biol. 312*, 1135−1160.
8. Pascher, T. (2001) Temperature and driving force dependence of the folding rate of reduced horse heart cytochrome *c*, *Biochemistry 40*, 5812−5820.
9. Arcovito, A., Gianni, S., Brunori, M., Travaglini-Allocatelli, C., and Bellelli, A. (2001) Fast coordination changes in cytochrome *c* do not necessarily imply folding, *J. Biol. Chem. 276*, 41073−41078.
10. Hagen, S. J., Latypov, R. F., Dolgikh, D. A., and Roder, H. (2002) Rapid intrachain binding of histidine-26 and histidine-33 to heme in unfolded ferrocytochrome *c*, *Biochemistry 41*, 1372−1380.
11. Chen, E., Goldbeck, R. A., and Kliger, D. S. (2003) Earliest events in protein folding: Submicrosecond secondary structure formation in reduced cytochrome *c*, *J. Phys. Chem. A 107*, 8149−8155.
12. Chen, E., Goldbeck, R. A., and Kliger, D. S. (2004) The earliest events in protein folding: A structural requirement for ultrafast folding in cytochrome *c*, *J. Am. Chem. Soc. 126*, 11175−11181.
13. Kumar, R., Prabhu, N. P., and Bhuyan, A. K. (2005) Ultrafast events in the folding of ferrocytochrome *c*, *Biochemistry 44*, 9359−9367.
14. Elöve, G. A., Chaffotte, A. F., Roder, H., and Goldberg, M. E. (1992) Early steps in cytochrome *c* folding probed by time-resolved circular dichroism and fluorescence spectroscopy, *Biochemistry 31*, 6876−6883.
15. Abel, C. J., Goldbeck, R. A., Latypov, R. F., Roder, H., and Kliger, D. S. (2007) Conformational equilibration time of unfolded protein chains and the folding speed limit, *Biochemistry 46*, 4090−4099.
16. Babul, J., and Stellwagen, E. (1971) The existence of heme-protein coordinate-covalent bonds in denatured solvents, *Biopolymers 10*, 2359−2361.
17. Elöve, G. A., Bhuyan, A. K., and Roder, H. (1994) Kinetic mechanism of cytochrome *c* folding: Involvement of the heme and its ligands, *Biochemistry 33*, 6925−6935.
18. Colón, W., Wakem, L. P., Sherman, F., and Roder, H. (1997) Identification of the predominant non-native histidine ligand in unfolded cytochrome *c*, *Biochemistry 36*, 12535−12541.
19. Thomas, Y. G., Goldbeck, R. A., and Kliger, D. S. (2000) Characterization of equilibrium intermediates in denaturant-induced unfolding of ferrous and ferric cytochromes *c* using magnetic circular dichroism, circular dichroism, and optical absorption spectroscopies, *Biopolymers 57*, 29−36.
20. Goldbeck, R. A., Thomas, Y. G., Chen, E., Esquerra, R. M., and Kliger, D. S. (1999) Multiple pathways on a protein-folding energy landscape: Kinetic evidence, *Proc. Natl. Acad. Sci. U.S.A. 96*, 2782−2787.
21. Pollock, W. B. R., Rosell, F. I., Twitchett, M. B., Dumont, M. E., and Mauk, A. G. (1998) Bacterial expression of a mitochondrial cytochrome *c*. Trimethylation of lys72 in yeast iso-1-cytochrome *c* and the alkaline conformational transition, *Biochemistry 37*, 6124−6131.
22. Rosell, F., and Mauk, A. G. (2002) Spectroscopic properties of a mitochrondrial cytochrome *c* with a single thioether bond to the heme prosthetic group, *Biochemistry 41*, 7811−7818.
23. Rumbley, J. N., Hoang, L., and Englander, S. W. (2002) Recombinant equine cytochrome *c* in *Escherichia coli*: High-level expression, characterization, and folding and assembly mutants, *Biochemistry 41*, 13894−13901.
24. Shapiro, D. B., Goldbeck, R. A., Che, D., Esquerra, R. M., Paquette, S. J., and Kliger, D. S. (1995) Nanosecond optical rotatory dispersion spectroscopy: Application to photolyzed hemoglobin-CO kinetics, *Biophys. J. 68*, 326−334.
25. Vickery, L., Nozawa, T., and Sauer, K. (1976) Magnetic circular dichroism studies of low-spin cytochromes. Temperature dependence and effects of axial coordination on the spectra of cytochrome *c* and cytochrome b_5, *J. Am. Chem. Soc. 98*, 351−357.
26. O'Connor, D. B., Goldbeck, R. A., Hazzard, J. H., Kliger, D. S., and Cusanovich, M. A. (1993) Time-resolved absorption and magnetic circular dichroism spectroscopy of cytochrome c_3 from *Desulfovibrio*, *Biophys. J. 65*, 1718−1726.
27. Wilgus, H., and Stellwagen, E. (1974) Alkaline isomerization of ferricytochrome *c*: identification of the lysine ligand, *Proc. Natl. Acad. Sci. U.S.A. 71*, 2892−2894.
28. Gadsby, P. M. A., Peterson, J., Foote, N., Greenwood, C., and Thomson, A. J. (1987) Identification of the ligand-exchange process in the alkaline transition of horse heart cytochrome *c*, *Biochem. J. 246*, 43−54.
29. Russell, B. S., Melenkivitz, R., and Bren, K. L. (2000) NMR investigation of ferricytochrome *c* unfolding: Detection of an equilibrium unfolding intermediate and residual structure in the denatured state, *Proc. Natl. Acad. Sci. U.S.A. 97*, 8312−8317.
30. Russell, B. S., and Bren, K. L. (2002) Denaturation dependence of equilibrium unfolding intermediates and denatured state structure of horse ferricytochrome *c*, *J. Biol. Inorg. Chem. 7*, 909−916.
31. Hammack, B., Godbole, S., and Bowler, B. E. (1998) Cytochrome *c* folding traps are not due solely to histidine-heme ligation: Direct demonstration of a role for N-terminal amino group-heme ligation, *J. Mol. Biol. 275*, 719−724.
32. Fisher, W. R., Taniuchi, H., and Anfinsen, C. B. (1973) On the role of heme in the formation of the structure of cytochrome *c*, *J. Biol. Chem. 248*, 3188−3195.
33. Stellwagen, E., Rysavy, R., and Babul, G. (1972) The conformation of horse heart apocytochrome *c*, *J. Biol. Chem. 247*, 8074−8077.
34. Kuroda, Y. (1993) Residual helical structure in the C-terminal fragment of cytochrome *c*, *Biochemistry 32*, 1219−1224.

35. Latypov, R. F., Cheng, H., Roder, N. A., Zhang, J., and Roder, H. (2006) Structural characterization of an equilibrium unfolding intermediate in cytochrome *c*, *J. Mol. Biol. 357*, 1009−1025.
36. Kurchan, E., Roder, H., and Bowler, B. E. (2005) Kinetics of loop formation and breakage in the denatured state of iso-1-cytochrome *c*, *J. Mol. Biol. 353*, 730−743.
37. Northey, J. G. B., Di Nardo, A. A., and Davidson, A. R. (2002) Hydrophobic core packing in the SH3 domain folding transition state, *Nat. Struct. Biol. 9*, 126−130.
38. Qin, W., Sanishvili, R., Plotkin, B., Schejter, A., and Margoliash, E. (1995) The role of histidines 26 and 33 in the structural stabilization of cytochrome *c*, *Biochim. Biophys. Acta 1252*, 87−94.
39. Sinibaldi, F., Piro, M. C., Howes, B. D., Smulevich, G., Ascoli, F., and Santucci, R. (2003) Rupture of the hydrogen bond linking two Ω-loops induces the molten globule state at neutral pH in cytochrome *c*, *Biochemistry 42*, 7604−7610.
40. Fetrow, J. S., Dreher, U., Wiland, D. J., Schaak, D. L., and Boose, T. L. (1998) Mutagenesis of histidine 26 demonstrates the importance of loop-loop and loop-protein interactions for the function of iso-1-cytochrome *c*, *Protein Sci. 7*, 994−1005.
41. Taler, G., Navon, G., and Becker, O. M. (1998) The interaction of borate ions with cytochrome *c* surface sites: A molecular dynamics study, *Biophys. J. 75*, 2461−2468.
42. Yamamoto, Y. (1997) A ^{1}H NMR study of structurally relevant inter-segmental hydrogen bond in cytochrome *c*, *Biochim. Biophys. Acta 1343*, 193−202.
43. Godbole, S., Hammack, B., and Bowler, B. E. (2000) Measuring denatured state energetics: Deviations from random coil behavior and implications for the folding of iso-1-cytochrome *c*, *J. Mol. Biol. 296*, 217−228.
44. Tanford, C. (1968) Protein denaturation, *Adv. Protein Chem. 23*, 121−282.
45. Pierce, M. M., and Nall, B. T. (2000) Coupled kinetic traps in cytochrome *c* folding: His-heme misligation and proline isomerization, *J. Mol. Biol. 298*, 955−969.
46. Hammack, B. N., Smith, C. R., and Bowler, B. E. (2001) Denatured state thermodynamics: Residual structure, chain stiffness and scaling factors, *J. Mol. Biol. 311*, 1091−1104.
47. Sivakolundu, S. G., and Mabrouk, P. A. (2003) Structure-function relationship of reduced cytochrome *c* probed by complete solution structure determination in 30% acetonitrile/water solution, *J. Biol. Inorg. Chem. 8*, 527−539.
48. Keilin, D. (1966) in *The history of cell respiration and cytochromes*, Cambridge University Press, New York.
49. Pettigrew, G. W., and Moore, G. R. (1987) in *Cytochromes c: Biological aspects*, Springer-Verlag, Berlin.
50. Jiang, X., and Wang, X. (2004) Cytochrome *c*-mediated apoptosis, *Annu. Rev. Biochem. 73*, 87−106.
51. Hiramatsu, K., and Yang, J. T. (1983) Cooperative binding of hexadecyltrimethylammonium chloride and sodium dodecyl sulfate to cytochrome *c* and the resultant change in protein conformation, *Biochim. Biophys. Acta 743*, 106−114.
52. de Jongh, H. H. J., Killian, J. A., and de Kruijff, B. (1992) A water-lipid interface induces a highly dynamic folded state in apocytochrome *c* and cytochrome *c*, which may represent a common folding intermediate, *Biochemistry 31*, 1636−1643.
53. Rankin, S. E., Watts, A., Roder, H., and Pinheiro, T. J. T. (1999) Folding of apocytochrome *c* induced by the interaction with negatively charged lipid micelles proceeds via a collapsed intermediate state, *Protein Sci. 8*, 381−393.
54. Oellerich, S., Wackerbarth, H., and Hildebrandt, P. (2003) Conformational equilibria and dynamics of cytochrome *c* induced by binding of sodium dodecyl sulfate monomers and micelles, *Eur. Biophys. J. 32*, 599−613.

BI7007273